Molecular Dynamics Thermal Conductivity Computation of a Quantum Cascade Laser Diode Super-Lattice

Kyle Horne,[1,2] *Thomas Antoni,*[2,3] *Sebastian Volz,*[2] *Mathieu Carras,*[4] *and Virginie Trinité*[4]

[1]Mechanical and Aerospace Engineering, Utah State University, Logan, UT 84322, USA

[2]Laboratoire d'Energétique Moléculaire et Macroscopique, Combustion, UPR CNRS 288, Ecole Centrale Paris, Grande Voie des Vignes, 92295 Châtenay-Malabry, France.

[3]École Centrale Paris, Laboratoire de Photonique Quantique et Moléculaire, CNRS (UMR 8537), École Normale Supérieure de Cachan, Grande Voie des Vignes, F-92295 Châtenay-Malabry cedex, France.

[4]THALES Research & Technology, Campus Polytechnique 1, avenue Augustin Fresnel 91767 Palaiseau cedex, France

Abstract

This paper reports work in which molecular dynamics are used to simulate a single cascade of a quantum cascade laser diode with the intent of computing the effective thermal conductivity in the cross-plane direction. The Tersoff potential is used with coefficients found from the literature for inter-atomic forces, and the Green-Kubo relation is used to compute the conductivity from the integral of the system heat flux autocorrelation. The computed conductivity lies in the same range as measurements found in the literature.

Introduction

Quantum cascade lasers (QCLs) represent a significant development in the area of band gap engineering[1], and although great advances have been achieved in terms of electronic transport and optical coupling, they still suffer from unoptimized thermal designs despite efforts to measure and optimize their thermal properties. Due to their high resistivity, quantum well structures are subject to an intense heating when high electrical powers are applied, as in the case of laser diodes, and their limited volume prevents an efficient heat evacuation. For this reason, thermal management of QCLs is a critical issue, and if it is usual to stabilize those lasers with a Peltier module, new technological designs are often proposed to drain the heat out of the structure; such attempts are buried structures[2, 3], or micro-stripe fabrication[4]. Heat has a dramatic impact on QCLs operation, not only because it can damage the diode, but also because it changes the effective optical index of the materials, which can result in a detuning of the optical mode with the electronic gain. An improved understanding of QCL phononics can lead to more optimized designs which can remove waste heat more effectively and more accurately couple electron and phonon modes. But also, a fine control of the diode's temperature is necessary to develop tunable structures.

Molecular dynamics simulations can provide detailed information about phonon activity and propagation, including thermal conductivity values and dispersion relations; the only limitations are the existence of an inter-atomic potential that adequately models atomic interactions and the normal limitations of classical physics when applied to atomic systems.

While several functional forms could be used for the inter-atomic potential, most previous work has used the Tersoff[5, 6, 7, 8] functional for this purpose. The potential is defined as the difference of repulsive (f_R) and attractive (f_A) potentials (equations 1,3-4), where A and B are energies of attraction and repulsion, while r_{ij} is the distance between the interaction atoms; the characteristic lengths of attraction and repulsion are λ_2 and λ_1 respectively. The attractive potential is multiplied by b_{ij}, which is a function of the bonding environment (equation 5), resulting in a three-body potential that can include angular effects such as those in III-IV semiconductor materials. The entire potential is controlled through a cutoff function $f_C(r)$ (equation 2) which allows for more efficient computation through the exclusion of negligible forces from distant atoms; the cutoff function smoothly transitions from one to zero using a sine function, with a mean effective range of R smoothed out over a distance D surrounding the cutoff. The bonding environment is modeled using the ζ_{ij} term (equation 6), which includes the distance between the bonding atoms and the third body (r_{ik}), as well as the angle formed by the three atoms (θ_{ijk}). This angle is the input to the function $g(\theta)$ (equation 7) which includes the empirically-fit parameters c, d, and $\cos\theta_0$. It should be noted that although $\cos(\theta_0)$ would be considered as the cosine of a constant angle, it is often found in coefficients as the parameter h and has a value

outside the range $[-1,1]$ that would be expected[9] for a parameter expressed as the cosine of an angle.

$$E = \frac{1}{2}\sum_i\sum_{i\neq j}\left[f_C\left(r_{ij}\right)\left(f_R\left(r_{ij}\right)-b_{ij}f_A\left(r_{ij}\right)\right)\right] \quad (1)$$

$$f_C(r) = \begin{cases} 1 & r < R-D \\ \frac{1}{2}-\frac{1}{2}\sin\left(\frac{\pi}{2}\frac{r-R}{D}\right) & R-D<r<R+D \\ 0 & r>R+D \end{cases} \quad (2)$$

$$f_R(r) = A\exp\left(-\lambda_1 r\right) \quad (3)$$

$$f_A(r) = B\exp\left(-\lambda_2 r\right) \quad (4)$$

$$b_{ij} = \left(1+\beta^n\zeta_{ij}^n\right)^{-\frac{1}{2n}} \quad (5)$$

$$\zeta_{ij} = \sum_{k\neq i,j}\left[f_C\left(r_{ik}\right)g\left(\theta_{ijk}\right)\exp\left(\lambda_3^m\left(r_{ij}-r_{ik}\right)^m\right)\right] \quad (6)$$

$$g(\theta) = 1+\frac{c^2}{d^2}-\frac{c^2}{d^2+\left(\cos\theta-\cos\theta_0\right)^2} \quad (7)$$

Due to the previous success seen from its use, the Tersoff functional was used to compute inter-atomic potentials with coefficients for all interactions besides those involving aluminum taken from the work of Nordlund[10]; the coefficients involving aluminum were constructed from the work of Sayed[11] and extended to all the required combinations using the mixing model proposed by Tersoff. Examination of the III-III coefficients from Nordlund suggest that this same mixing model was used as a starting point for those coefficients before minor modification as well.

The molecular dynamics simulations were run using the Lammps[1] software developed primarily at Sandia National Laboratories[12]. Since the Tersoff potential is already included in Lammps, no changes to the code were necessary for the present work; the code was compiled and run on USU's Division of Research Computing clusters with little difficulty. Due to the need for many simulation trajectories, the simulation setup process was automated in the form of several Python scripts.

The active region of QCLs is typically composed of a repetition (about 50 times) of a seminal period, the cascade, where GaInAs (well), AlInAs (barrier) layers are alternated with a varying thickness on the order of few mono-atomic layers as presented in table (1). We expect their thermal conductivity along the growth axis to be different from the bulk InAs one for at least two reasons. First, the layers are made of allows associating InAs with an atoms of very different weights (Ga or Al). Then the nanolayering will have an influence on the phonon propagation. Since the cascade is few hundred nanometers in height, that is very large compared to the phonons mean free path, it is reasonable to focus on only one period.

Methods

First, a script constructs the QCL structure by looping through all sites in the lattice and placing an atom appropriate for the location. This is determined by position according to the layer structure of the QCL, which is smoothed slightly to model some natural atomic diffusion during the deposition process. Since many QCLs are not designed with a perfect periodic structure, a weighted average of all the periods in the QCL of interest was computed for the layer structure. Figure (1) presents the data used to select the atoms for each lattice site.

Tab. 1: Typical QCL structure

#	III-IV	l [Å]	#	III-IV	l [Å]
1	GaInAs	35.8	9	GaInAs	21.0
2	AlInAs	14.1	10	AlInAs	14.6
3	GaInAs	34.4	11	GaInAs	47.7
4	AlInAs	18.5	12	AlInAs	8.4
5	GaInAs	32.6	13	GaInAs	51.5
6	AlInAs	25.7	14	AlInAs	9.7
7	GaInAs	30.8	15	GaInAs	44.2
8	AlInAs	37.6	16	AlInAs	12.0

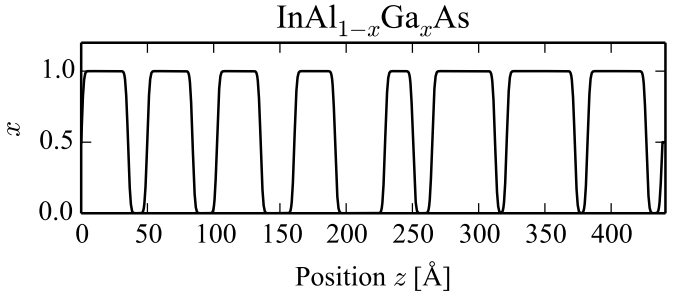

Fig. 1: A slice of the computational domain showing the layered structure of a single QCL period

The first script also creates a 'include' file used by the Lammps script to provide random number seeds for velocity initialization and also provide the simulation with other details of the system setup. A second script generates the coefficients file used by Lammps for the Tersoff potential, taking the data from literature and formatting it appropriately. This was initially done to allow the coefficients to be systematically altered for fitting, but also allows Tersoff mixing to be computed dynamically. Lammps is then run using the constructed system.

After initialization, the system is relaxed in the NTP (constant number of atoms, temperature, and pressure) regime for 20 ps to allow the system to adjust to the potential, since the Python script generates it with a prescribed lattice parameter. Next, the system is equilibrated in NVE (constant number of atoms, volume and energy) for 200 ps to adjust to the correct velocity distributions and remove artifacts of the initialization. Lastly, the system is run for another 1600 ps in NVE during

[1] `http://lammps.sandia.gov`

Tab. 2: Fit parameters

Material	A [eV^{2}ps^{-2}Å^{-4}]	τ [ps]	p
AlAs	1.29×10^{-5}	77.4	0.86
GaAs	4.43×10^{-6}	18.0	0.98
InAs	2.66×10^{-6}	38.1	0.95
InGaAs	2.46×10^{-7}	2.64	0.65
InAlAs	1.73×10^{-7}	2.03	0.31

which the system heat flux is computed and recorded to a file after Lammps corrects it to remove the effects of bulk motion.

The integrated autocorrelation of the system heat flux can be used to compute the thermal conductivity in a particular direction i as given in equation (8), where V is the system volume, T is the system temperature, $\langle J_i(0) J_i(t)\rangle$ is the ensemble heat flux autocorrelation, and k_B is the Boltzmann constant.[13, 14, 15, 16, 17].

$$k_i = \frac{V}{k_B T^2}\int_0^\infty \langle J_i(0) J_i(t)\rangle \, dt \tag{8}$$

Because of the random nature of the simulations, the ensemble average of the autocorrelation is what must be integrated, and to this end nearly one hundred simulations were run with different initial velocities to provide independent trajectories. Each simulation's heat flux was autocorrelated independently, and then the average of all the autocorrelations was computed. This average autocorrelation was then numerically integrated, and equation (9) was fit against the result.

$$I = A\left[1 - e^{-(t/\tau)^p}\right] \tag{9}$$

This expression was selected since its functional form closely matches the results of the simulations. The fit parameter A is the asymptotic plateau value of the expression, while τ is the characteristic time to approach that value and p is the exponential order of that approach. The units on A are in energy flux squared (SI equivalent: $\left[W/m^2\right]^2$), while the units of τ are time and the parameter p is without units. Table 2 summarizes the fit parameters for the materials considered in this work.

Before considering the results for the QCL, we checked that our simulations give correct estimates of the thermal conductivity of standard III-V compounds that enter QCLs growth such as InAs and GaAs, and also compute the thermal conductivity of the two alloys GaInAs and AlInAs. The results are presented in Table 3, computed from the parameters from Table 2. These simulations follow the same general procedure as that presented for the QCL, but with smaller systems and for shorter times; the longer times and larger system are required for the QCL due to its complexity.

As can be seen from the table, none of the MD predictions deviate from experimental values by more than 60%, which is quite remarkable when the nature of MD simulation is considered. The results for InAs are considerably more accurate than

Tab. 3: Predicted and measured thermal conductivies

III-IV Material	Experimental k [$W/m\cdot K$]	Computed k[$W/m\cdot K$]	Difference [%]
AlAs	80 [18]	106	+32
GaAs	55 [19]	35.8	-35
InAs	27 [19]	26.4	-2
GaInAs	5 [20]	2.2	-56
AlInAs	3.5 [21]	1.6	-54

would be expected, while the AlAs and GaAs are more like conventional MD results. Unsurprisingly, the alloys AlInAs and GaInAs show the worst agreement with experimental values, but they also involve the most empirically-determined coefficients for the inter-atomic potentials; it is believed that most uncertainty in the simulation results are a direct consequence of inaccuracy of the potential used. Also as expected, the alloys show lower thermal conductivities than the non-alloyed materials.

Given the data presented in Table 3, we expect the error in thermal conductivities computed from these potentials to be no worse than 50-75%, which may seem like a large range, but it is still reasonable for a result from atomic simulation.

Results

Figure 2 shows the flux autocorrelation integral for the QCL system described previously, as well as the curve resulting from fitting equation 9 to the simulation data. The parameters from the curve fit can be found in Table 4, where the value of p is unsurprisingly found to be closer to the values for alloys than pure materials. The longer characteristic time can be explained by considering the very small structures that should damp out faster oscillations, leaving only the long-time oscillations to carry energy. It is also interesting that the simulation predicts a thermal conductivity larger than those of the constituent materials.

The effective bulk thermal conductivities of QCL structures similar to the one simulated in this work have been previously measured by other using a combination of temperature measurements and finite element analysis; these results can be found in the works of Scamarcio[22], Vitiello[23, 24] and Evans[25], and report values in the range $k = [2, 8]$ W/m $\cdot$ K . Considering that the coefficients used for our simulations were developed primarily from mechanical properties, this agree-

Tab. 4: QCL results

A [eV^{2}ps^{-2}Å^{-4}]	τ [ps]	p	k [W m^{-1}K^{-1}]
1.13×10^{-7}	61.7	0.49	5.9

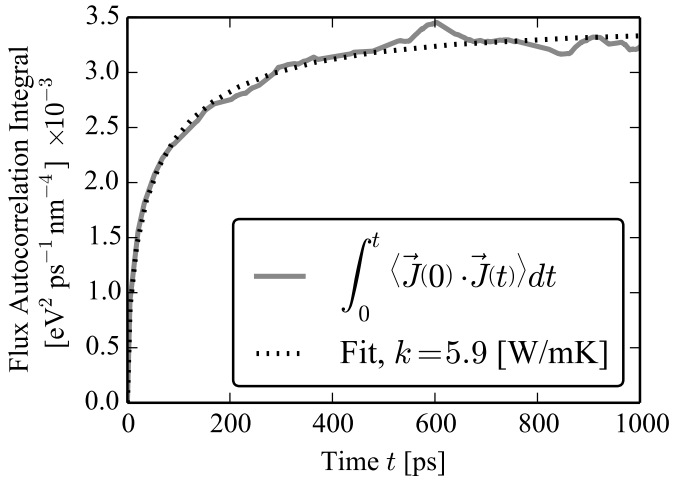

Fig. 2: QCL flux autocorrelation integral

ment between simulation and experiment is remarkable.

Conclusions

While the present work suggests that molecular dynamics results can agree quite well with experimental values, the real advantage of the present work is all the additional information available from a simulation. Since the thermal conductivities agree so well with experiment, the phonon properties can be trusted enough to drive new QCL designs that take better advantage of the phonon band structures and how they compare with those of the electrons. More work is to be done computing the in-plane conductivity as well as examining the phonon dispersion relationships.

References

[1] Jerome Faist, Federico Capasso, Deborah L. Sivco, Alfred Y. Cho, and Albert L. Hutchinson Carlo Sirtori. Quantum cascade laser. *Science*, 264:553–556, April 1994.

[2] Mattias Beck, Daniel Hofstetter, Thierry Aellen, Jérôme Faist, Ursula Oesterle, Marc Ilegems, Emilio Gini, and Hans Melchior. Continuous wave operation of a mid-infrared semiconductor laser at room temperature. *Science*, 295(5553):301–305, 2002.

[3] Manijeh Razeghi, Neelanjan Bandyopadhyay, Yanbo Bai, Quanyong Lu, and Steven Slivken. Recent advances in mid infrared (3-5 μm) quantum cascade lasers. *Opt. Mater. Express*, 3(11):1872–1884, Nov 2013.

[4] G. M. de Naurois, B. Simozrag, G. Maisons, V. Trinite, F. Alexandre, and M. Carras. High thermal performance of μ-stripes quantum cascade laser. *Applied Physics Letters*, 101(4):–, 2012.

[5] J Tersoff. New empirical model for the structural properties of silicon. *Physical Review Letters*, 56(6):632–635, 1986.

[6] J Tersoff. New empirical approach for the structure and energy of covalent systems. *Physical Review B*, 37(12):6991, 1988.

[7] J Tersoff. Empirical interatomic potential for silicon with improved elastic properties. *Physical Review B*, 38:9902–9905, 1988.

[8] J Tersoff et al. Modeling solid-state chemistry: Interatomic potentials for multicomponent systems. *Physical Review B*, 39(8):5566–5568, 1989.

[9] Roger Smith. A semi-empirical many-body interatomic potential for modelling dynamical processes in gallium arsenide. *Nuclear Instruments and Methods in Physics Research Section B: Beam Interactions with Materials and Atoms*, 67(1):335–339, 1992.

[10] K Nordlund, J Nord, J Frantz, and J Keinonen. Strain-induced kirkendall mixing at semiconductor interfaces. *Computational materials science*, 18(3):283–294, 2000.

[11] M Sayed, JH Jefferson, AB Walker, and AG Cullis. Computer simulation of atomic displacements in si, GaAs, and alas. *Nuclear Instruments and Methods in Physics Research Section B: Beam Interactions with Materials and Atoms*, 102(1):232–235, 1995.

[12] Steve Plimpton. Fast parallel algorithms for short-range molecular dynamics. *Journal of Computational Physics*, 117(1):1–19, 1995.

[13] Ryogo Kubo. Statistical-mechanical theory of irreversible processes. i. general theory and simple applications to magnetic and conduction problems. *Journal of the Physical Society of Japan*, 12(6):570–586, 1957.

[14] Ryogo Kubo, Mario Yokota, and Sadao Nakajima. Statistical-mechanical theory of irreversible processes. ii. response to thermal disturbance. *Journal of the Physical Society of Japan*, 12(11):1203–1211, 1957.

[15] Sebastian G Volz and Gang Chen. Molecular dynamics simulation of thermal conductivity of silicon nanowires. *Applied Physics Letters*, 75(14):2056–2058, 1999.

[16] Sebastian G Volz and Gang Chen. Molecular-dynamics simulation of thermal conductivity of silicon crystals. *Physical Review B*, 61(4):2651, 2000.

[17] S Volz, JB Saulnier, G Chen, and P Beauchamp. Computation of thermal conductivity of si/ge superlattices by molecular dynamics techniques. *Microelectronics Journal*, 31(9):815–819, 2000.

[18] A. Katz. *Indium phosphide and related materials: processing, technology, and devices*. Artech House Materials Library. Artech House, 1992.

[19] PD Maycock. Thermal conductivity of silicon, germanium, iii–v compounds and iii–v alloys. *Solid-state electronics*, 10(3):161–168, 1967.

[20] Sadao Adachi. Lattice thermal resistivity of iii-v compound alloys. *Journal of Applied Physics*, 54(4):1844–1848, 1983.

[21] SL Singer, W Kim, A Majumdar, JMO Zide, and AC Gossard. Thermal conductivity measurements of eras: Ingaalas for thermoelectric applications. In *The Sixth International Workshop on Micro and Nanotechnology for Power Generation and Energy Conversion Applications*, November 2006.

[22] Vincenzo Spagnolo, Antonia Lops, Gaetano Scamarcio, Miriam S Vitiello, and Cinzia Di Franco. Improved thermal management of mid-IR quantum cascade lasers. *Journal of Applied Physics*, 103(4):043103–043103, 2008.

[23] Miriam S Vitiello, Gaetano Scamarcio, Vincenzo Spagnolo, Antonia Lops, Quankui Yang, Christian Manz, and Joachim Wagner. Experimental investigation of the lattice and electronic temperatures in gainas/ AlGaAssb quantum-cascade lasers. *Applied physics letters*, 90:121109, 2007.

[24] Miriam S Vitiello, Tobias Gresch, Antonia Lops, Vincenzo Spagnolo, Gaetano Scamarcio, Nicolas Hoyler, Marcella Giovannini, and Jérôme Faist. Influence of inas, alas δ layers on the optical, electronic, and thermal characteristics of strain-compensated gainas/alinas quantum-cascade lasers. *Applied Physics Letters*, 91(16):161111–161111, 2007.

[25] Craig A Evans, Dragan Indjin, Zoran Ikonic, Paul Harrison, Miriam Serena Vitiello, Vincenzo Spagnolo, and Gaetano Scamarcio. Thermal modeling of terahertz quantum-cascade lasers: comparison of optical waveguides. *Quantum Electronics, IEEE Journal of*, 44(7):680–685, 2008.